Applied Catalysis B: Environmental 334 (2023) 122865

Contents lists available at ScienceDirect

Applied Catalysis B: Environmental

journal homepage: www.elsevier.com/locate/apcatb

Charge separation via synergy of homojunction and electrocatalyst in $BiVO_4$ for photoelectrochemical water splitting

Zifei Xie [a], Daoming Chen [a], Jingtong Zhai [a], Yongchao Huang [a,*], Hongbing Ji [b,*]

[a] Institute of Environmental Research at Greater Bay Area, Key Laboratory for Water Quality and Conservation of the Pearl River Delta, Ministry of Education, Guangzhou University, Guangzhou 510006, China

[b] Institute of Green Petroleum Processing and Light Hydrocarbon Conversion, College of Chemical Engineering, Zhejiang University of Technology, Hangzhou 310014, China

ARTICLE INFO

Keywords:
$BiVO_4$
Nanodots
Charge separation
Crystal facet
Photoelectrochemical water splitting

ABSTRACT

Bismuth vanadate ($BiVO_4$) as oxygen evolution photoanodes in photoelectrochemical (PEC) water splitting is hampered by the severe charge recombination and sluggish kinetic reaction. Herein, we successively construct a novel homogenous BVO/$BiVO_4$ photoanodes consisting of $BiVO_4$ nanodots (BVO) with exposed (011) crystal facet on $BiVO_4$ substrate that did not only creates tunable (011)/(110) crystal planes upon homogeneous interfacial contact but also demonstrates an unprecedented photocurrent density with outstanding performance. Theoretical calculations clearly reveal that the tunable (011)/(110) crystal facet facilitates the charge separation efficiency and water splitting kinetics. Furthermore, the photocurrent density of the homogenous BVO/$BiVO_4$ is further enhanced by additional photo-deposition of $NiFeO_x$ electrocatalyst layer (denoted $NiFeO_x$/BVO/$BiVO_4$). Consequently, the optimized $NiFeO_x$/BVO/$BiVO_4$ photoanodes not only reaches an unprecedented photocurrent density of 6.40 mA cm^{-2} at 1.23 V versus reversible hydrogen electrode (RHE) under simulated AM 1.5G illumination, but also generates an outstanding durability. This work endows a new environmentally friendly and effective path for improving PEC water splitting of $BiVO_4$ photoanodes.

1. Introduction

Replacing fossil fuels with clean energy is one of the most effective strategies to achieve carbon neutrality in the next coming decade [1,2]. Hydrogen (H_2) as a renewable and pollution-free energy has attracted significant attention in energy conversion research [3–5]. Photoelectrochemical (PEC) water splitting directly uses solar energy to dissociate water (H_2O) into H_2 and oxygen (O_2) through light-absorbing electrodes [1,6,7]. Thanks to bismuth vanadate ($BiVO_4$) as a promising photoanode for PEC water oxidation because of its high theoretical photocurrent of 7.5 mA cm^{-2} under AM 1.5 G illumination (100 mW cm^{-2}), suitable band structure and excellent light absorption capacity [8–11]. However, severe charges recombination in the bulk phase and surface of $BiVO_4$ hinders the efficacy of electrons and holes utilization, leading to unsatisfactory PEC performance [12–14].

Recent studies on $BiVO_4$ crystal facet engineering via different synthetic processes are promising photocatalysts for water oxidation [15–18]. The different $BiVO_4$ facet engineering shows that different crystal facets have great differences for the attraction of photogenerated electrons and holes, which can effectively enhance the charge separation [7,19–21]. For instance, Kim et al. [22] revealed that the exposed (040) facet $BiVO_4$ increased the charge separation and surface charge efficiencies, causing high photocurrent density of 0.94 mA cm^{-2}. Li et al. [23] reported that predominant (010) orientated $BiVO_4$ displayed a 2.9 times increment in PEC photocurrent than that of the (121) orientated $BiVO_4$. The experimental results showed that the electron movement in the (010) plane is higher and faster than that of (121) plane, causing a higher charge separation efficiency and PEC performance of (010) orientated $BiVO_4$. Nevertheless, the PEC properties of the $BiVO_4$-crystal facet-based photoanodes are still not comparable to the theoretical $BiVO_4$ value (7.5 mA cm^{-2} at 1.23 V). One of the possible reasons is the insufficient charge separation efficiency. A recent approach of introducing heterogeneous-based $BiVO_4$ (010)/g-C_3N_4 to enhance the charge separation efficiency has further improved the current density to 1.98 mA cm^{-2} at 1.23 V [24]. However, these $BiVO_4$ heterogeneous-based photocatalysts will form some interfaces, which will introduce defects and act as recombination centers and carrier traps during PEC water splitting [25–27]. Moreover, owing to the synergy between $BiVO_4$ and

* Corresponding authors.
E-mail addresses: huangych@gzhu.edu.cn (Y. Huang), jihb@mail.sysu.edu.cn (H. Ji).

https://doi.org/10.1016/j.apcatb.2023.122865
Received 9 February 2023; Received in revised form 12 April 2023; Accepted 8 May 2023
Available online 9 May 2023

other photocatalysts or co-catalysts in water oxidation, the hybrid may not be able to fully take the advantage of the entire catalyst's active surface area.

Alternatively, we aimed to enhance the charge separation kinetics for $BiVO_4$ via homojunction engineering. Herein, we enhance the charge separation efficiency of $BiVO_4$ water oxidation by photo-electrodepositing $BiVO_4$ nanodots (BVO) on $BiVO_4$ worm-like grain morphology matrix, with tunable (110) and (011) crystal facets, and systematically explain the mechanism of (011)/(110) crystal plane for promoted water oxidation. The integration of the BVO nanodots effectively improves the transmission of photogenerated electrons by reducing the diffusion distance and agglomerate due to high surface energy, leading to the reduction of performance and a poor stability [28–30]. Theoretical calculations show that the homojunction formed (011)/(110) crystal facet not only enhances the interfacial charge carrier dynamics, but also lowers the Gibbs free energy barrier of water oxidation, improves charge transfer and separation efficiencies. Subsequently, $NiFeO_x$ electrocatalyst was further photo-electrodeposited on $BVO/BiVO_4$ homojunction not only to enhance water oxidation kinetics but also improve the stability. The optimized $NiFeO_x/BVO/BiVO_4$ photoanodes demonstrated superior photocurrent density (6.40 mA cm^{-2}), high charge separation (95.4 %) and surface charge transfer efficiency (89.3 %) at 1.23 V vs. RHE. As a result, we provide a simple and viable strategy for designing excellent $BiVO_4$ photoanode for promoting solar energy conversion.

2. Experimental section

2.1. Synthesis of $BiVO_4$-based photoanodes

Pristine $BiVO_4$ photoanode was obtained by using our reported method [31]. Firstly, BiOI were electrodeposited on the fluorine doped tin oxide (FTO) from a solution containing 0.04 M $Bi(NO_3)_3{\cdot}xH_2O$ (98 %, Sigma-Aldrich), 0.4 M KI (98 %, Sigma-Aldrich) and 0.23 M *p*-benzoquinone (98 %, Sigma-Aldrich) at − 0.1 V vs. Ag/AgCl for 120 s. Subsequently, 200 μL dimethyl sulfoxide (98 %, Sigma-Aldrich) solution containing 0.2 M vanadyl acetylacetonate (98 %, Sigma-Aldrich) was added on the BiOI and then calcined at 450 °C for 120 min. The samples were steeped in 1 M NaOH solution to remove the redundant V_2O_5 and washed with water and ethanol. $BVO/BiVO_4$ homojunction photoanodes were obtained by electroplating bismuth vanadate nanodots (BVO) on the prepared $BiVO_4$ photoanodes. 0.03 M $Bi(NO_3)_3{\cdot}5H_2O$ (98 %, Sigma-Aldrich) and 0.03 M $VOSO_4$ (98 %, Sigma-Aldrich) were completely dissolved in 50 mL HNO_3 solution (pH = 0.5) (98 %, Sigma-Aldrich). Then using 3 M CH_3COONa (98 %, Sigma-Aldrich) solution to adjust the solution to pH = 4.7. Let the solution rise to 80 °C and stir for 60 min, electrodeposition was performed for 10 s at 1.95 V vs. Ag/AgCl and washed with deionized water. $NiFeO_x/BVO/BiVO_4$ photoanodes were prepared using a photoelectrodeposition method with a 0.4 M $FeSO_4$ (98 %, Sigma-Aldrich) and 0.04 M $NiSO_4$ (98 %, Sigma-Aldrich) solutions at 0.6 V vs. Ag/AgCl for 5 min

2.2. Characterization

The phase and structure of the prepared photoanodes were examined using X-ray diffraction (XRD, Supernova, Rigaku), UV–vis–NIR spectrophotometer (Lambda950, PerkinElmer), X-ray photoelectron spectroscope (XPS, ESCALAB250, Thermo-VG Scientific) and photoluminescence spectrometer (PL, Edinburgh FLS1000). The morphology of the samples was tested using transmission electron microscope (TEM, FEI Tecnai G2 F30) and field-emission scanning electron microscope (SEM, Gemini SEM 500).

2.3. Photoelectrochemical measurement

All the photoelectrochemical measurements were test in a three-electrode cell with a CHI660E electrochemical workstation (Shanghai). A Pt electrode, Ag/AgCl electrode and prepared photoelectrodes were used as counter electrode, reference electrode and working electrode, respectively. A Xenon lamp (PLS-FX300HU, Beijing Perfectlight) equipped with AM 1.5 G filters to obtain the 100 mW cm^{-2} light intensity. The electrolyte is a 0.5 M borate buffer solution at a pH value of 9.5 and 0.5 M Na_2SO_3 is used as holes scavenger. The formula involved in the paper is as follows:

$$E\ (\text{vs·RHE}) = E\ (\text{vs·Ag/AgCl}) + E_{\ \text{Ag/AgCl}}\ (\text{reference}) + 0{\cdot}0591\ \text{V} \times \text{pH} \quad (1)$$

$$ABPE = \frac{J_{H_2O} \times (1.23 - V_{\text{app}})}{P_{\text{light}}} \times 100\% \quad (2)$$

$$IPCE = \frac{1240}{\lambda} \times \frac{J_{\text{light}} - J_{\text{dark}}}{P_{\lambda}} \times 100\% \quad (3)$$

$$\eta_{transfer} = \frac{J_{H_2O}}{J_{Na_2SO_3}} \times 100\% \quad (4)$$

$$\eta_{sep} = \frac{J_{Na_2SO_3}}{J_{abs}} \times 100\% \quad (5)$$

Where, E_{RHE} is the potential vs. RHE. $E_{\ \text{Ag/AgCl}}$ (reference) is 0.197 V 25 °C and E (vs. Ag/AgCl) is the potential vs. Ag/AgCl. J_{H2O} is the photocurrent density, V_{app} is the applied external potential vs. RHE, P_{light} is the power density of the illumination (100 mW cm^{-2}). λ and P_{λ} are the incident light wavelength (nm) and the power density obtained at a specific wavelength (mW cm^{-2}), respectively.

3. Results and discussion

3.1. Physical and morphological characterization

The synthetic procedure of the $NiFeO_x/BVO/BiVO_4$ photoanode is illustrated in Fig. 1a. Generally, $BiVO_4$ nanodots were electroplated on pristine $BiVO_4$ photoanodes (denoted $BVO/BiVO_4$). Subsequently, the $NiFeO_x$ electrocatalyst layer was also photo-electrodeposited on the $BVO/BiVO_4$ photoanodes and denoted as $NiFeO_x/BVO/BiVO_4$. To observe the changes in the structure and phases of the prepared photoanodes, the crystal structure of samples was performed by X-ray diffraction (XRD). As shown in Fig. 1b, except for the diffraction peak of FTO substrates (SnO_2, JCPD#46-1088), all the other diffraction peaks correspond to the monoclinic $BiVO_4$ (JCPDS#14-0688) [31,32]. Interestingly, as shown in the inset of Fig. 1b, the intensity of (110) and (011) crystal facets have significant changes. This indicates that the loading of the BVO nanodots effectively enhances the intensity of the (011) crystal plane. For comparison, the XRD spectra of the pristine BVO was displayed in Fig. S1, confirming that (011)/(110) crystal plane was successfully constructed.

The scanning electron microscopy (SEM) images of $BiVO_4$-based photoanodes clearly demonstrate that $BiVO_4$-based photoanodes were worm-like grain morphology (Fig. S2, Supporting Information). Compared to pristine $BiVO_4$ (Fig. S3, Supporting Information), the typical transmission electron microscopy (TEM) image of $BVO/BiVO_4$ also displays worm-like grain morphology. Fig. S4 displayed the TEM image of $BVO/BiVO_4$ photoanode. Some particles about 10 nm diameter appeared on the surface of $BiVO_4$. High-resolution TEM (HRTEM) image collected from the surface of $BVO/BiVO_4$ revealed lattice fringes of 0.46 and 0.47 nm, corresponding to (011) and (110) phase of $BiVO_4$. This result confirms the formation of (011)/(110) interfacial contact. Furthermore, $NiFeO_x/BVO/BiVO_4$ also displays worm-like grain morphology (Fig. 1c) in which BVO nanodots with about 10 nm diameter appeared on the surface of $BiVO_4$ (Fig. 1d). Fig. 1e illustrates the high-resolution TEM (HR-TEM) image of the $NiFeO_x/BVO/BiVO_4$ sample. Well-resolved lattice fringes of 0.46 nm and 0.47 nm were observed, which can be attributed to (011) and (110) crystal plane of monoclinic

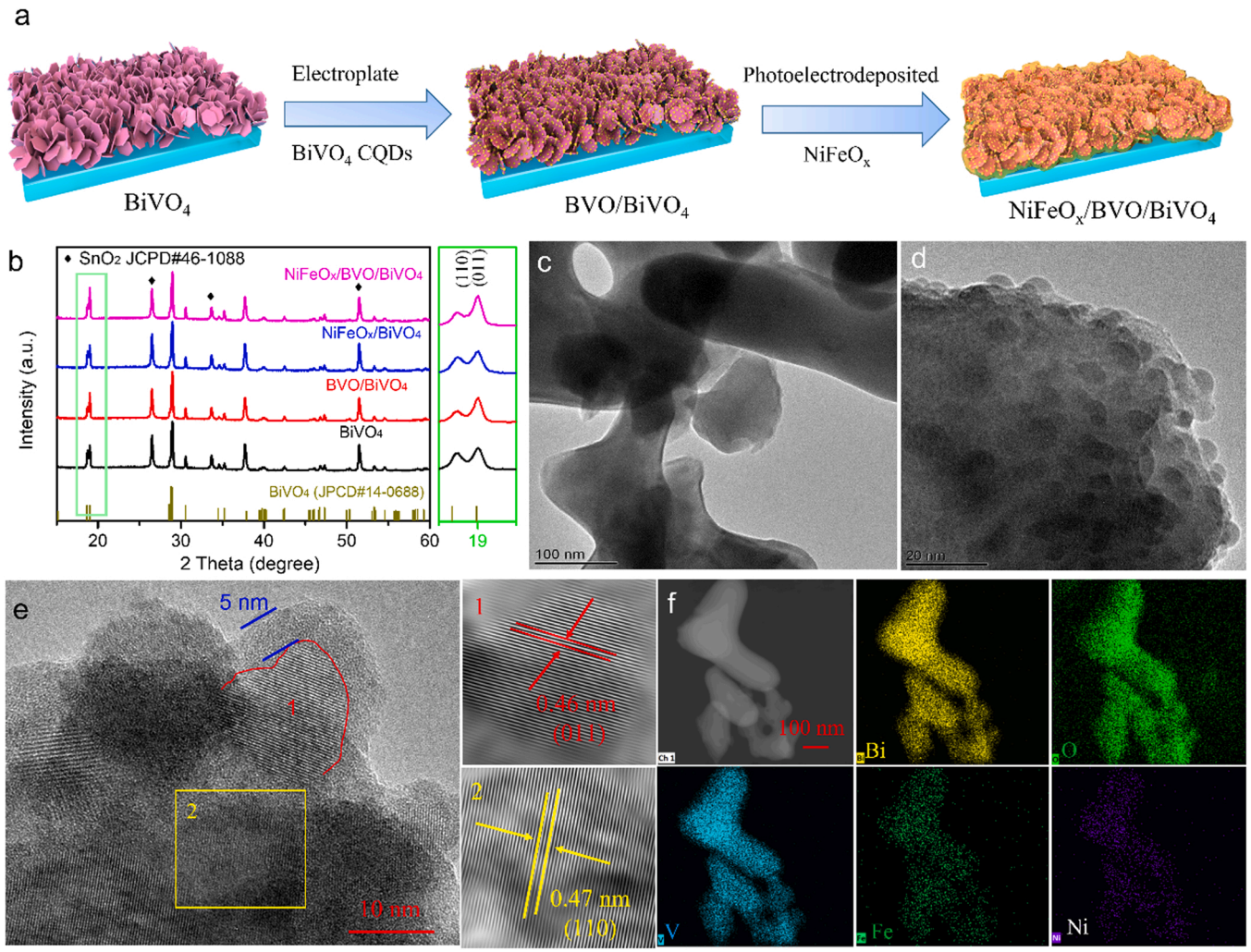

Fig. 1. (a) Schematic of the synthesis of $NiFeO_x$/BVO/$BiVO_4$ photoanodes. (b) XRD spectra of $BiVO_4$ based photoanodes. (c, d) TEM images, (e) HR-TEM images, and (f) elemental mapping of $NiFeO_x$/BVO/$BiVO_4$ photoanodes.

$BiVO_4$ (JCPDS#14–0688), indicating that BVO/$BiVO_4$ was successfully synthesized [33]. Furthermore, an ultrathin layer of about 5 nm covers the surface, suggesting that $NiFeO_x$ was successfully deposited on the surface of $NiFeO_x$/BVO/$BiVO_4$ sample. The elemental dispersive X-ray spectroscopy (EDX) images further illustrate the elemental composition of the $NiFeO_x$/BVO/$BiVO_4$ sample, and Bi, O, V, Fe, and Ni elements are evenly distributed within the entire catalyst (Fig. 1f).

To further confirm the surface compositions and elemental states of the $NiFeO_x$/BVO/$BiVO_4$ sample, X-ray photoelectron spectroscopy (XPS) test was carried out, and the results were displayed in Fig. 2. The high-resolution XPS displayed that the binding energy of the Bi 4f and V 2p of all samples did not shift, indicating that the phase and valence were not changed after electroplating (011) crystal of the crystal BVO, and also demonstrating the formation of $BiVO_4$ homojunction (BVO/$BiVO_4$). As shown in Fig. 2c, the high-resolution O 1s XPS were deconvoluted into three peaks, including lattice oxygen species (O_L), oxygen-deficient region (O_V), and dissociated oxygen species from water molecules (O_C) [1,34,35]. The formation of (011)/(110) crystal plane in BVO/$BiVO_4$ have not changed the oxygen's environment. Interestingly, the presence of $NiFeO_x$ electrocatalyst increases the dissociated oxygen species, which can facilitate the contact of the electrode with the solution. Furthermore, the signal of Fe and Ni were detected in $NiFeO_x$/BVO/$BiVO_4$ photoanodes, confirming that $NiFeO_x$ was successfully deposited on the surface of $NiFeO_x$/BVO/$BiVO_4$ sample (Fig. 2d).

3.2. Photoelectrochemical performance

To study the effect of (011)/(110) crystal plane towards promoting the water oxidation, the PEC properties of the pristine $BiVO_4$ and BVO/$BiVO_4$ photoanodes were first measured in 0.5 M borate buffer solution (pH = 9.5) under simulated AM 1.5G illumination. Under the back-side irradiation, the photocurrent density of BVO/$BiVO_4$ photoanode reaches 3.40 mA cm^{-2} at 1.23 V vs. RHE, which is much higher than that of pristine $BiVO_4$ (1.37 mA cm^{-2}), suggesting that the enhancement of the (011)/(110) crystal plane promotes water oxidation (Fig. 3a). While under front-side irradiation, the photocurrent densities of pristine $BiVO_4$ and BVO/$BiVO_4$ photoanodes decrease, compared with back-side irradiation. Therefore, the following PEC test was performed on the back-side irradiation. Upon the addition of $NiFeO_x$, the photocurrent densities of $NiFeO_x$/$BiVO_4$ and $NiFeO_x$/BVO/$BiVO_4$ increases up to 4.17 and 6.40 mA cm^{-2} at 1.23 V vs. RHE, respectively (Fig. 3b). Furthermore, $NiFeO_x$/BVO/$BiVO_4$ sample exhibits a negatively shifted onset potential to 0.2 V compared with $BiVO_4$ and BVO/$BiVO_4$ photoanodes (0.45 V), which contributed to the effectively separated the charge recombination [36,37]. Remarkably, the photocurrent density of $NiFeO_x$/BVO/$BiVO_4$ is much higher than most of the reported $BiVO_4$-based values with the same applied bias and electrolyte (Table S1, Supporting Information), confirming that $NiFeO_x$/BVO/$BiVO_4$ is an excellent photoanode for water oxidation.

The half-cell applied bias photon-to-current efficiencies (ABPEs)

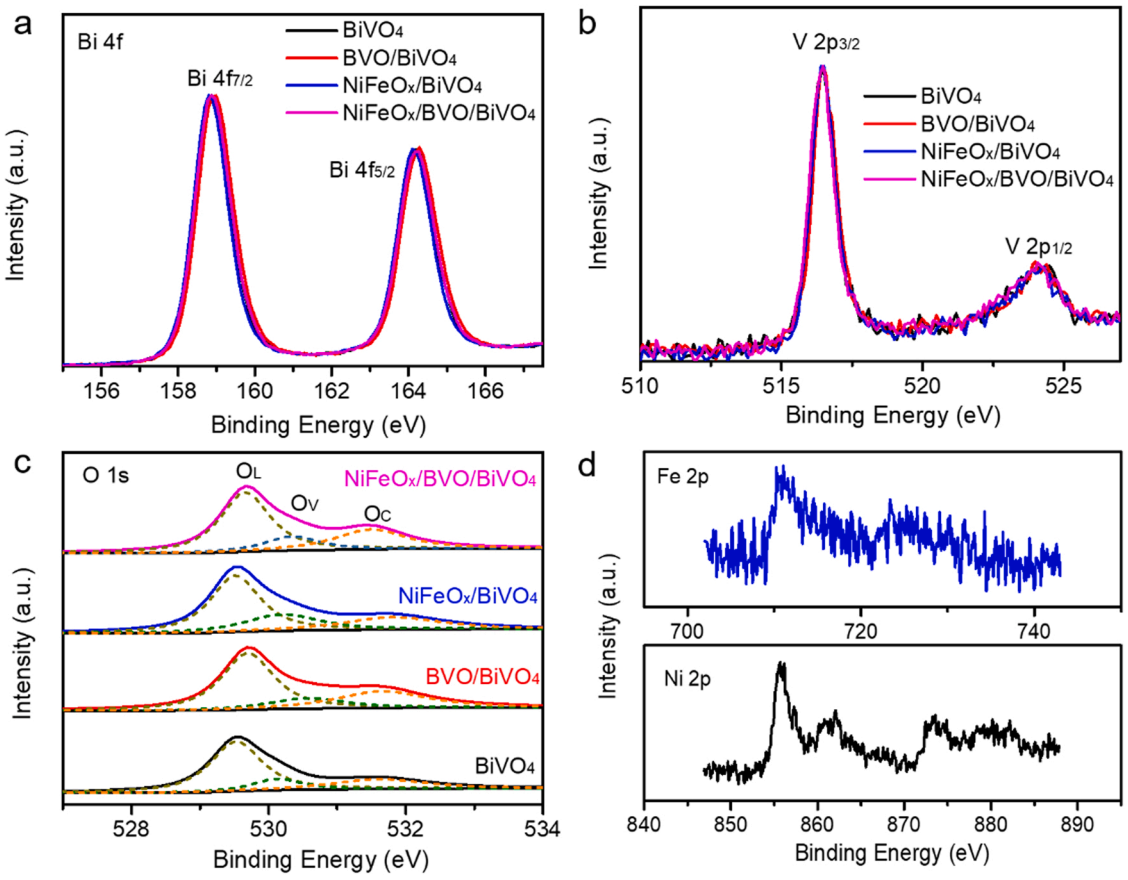

Fig. 2. (a) Bi 4f, (b) V 2p, and (c) O1s spectra of four $BiVO_4$ based photoanodes. (d) Fe 2p, Ni 2p spectra of $NiFeO_x/BVO/BiVO_4$ photoanode.

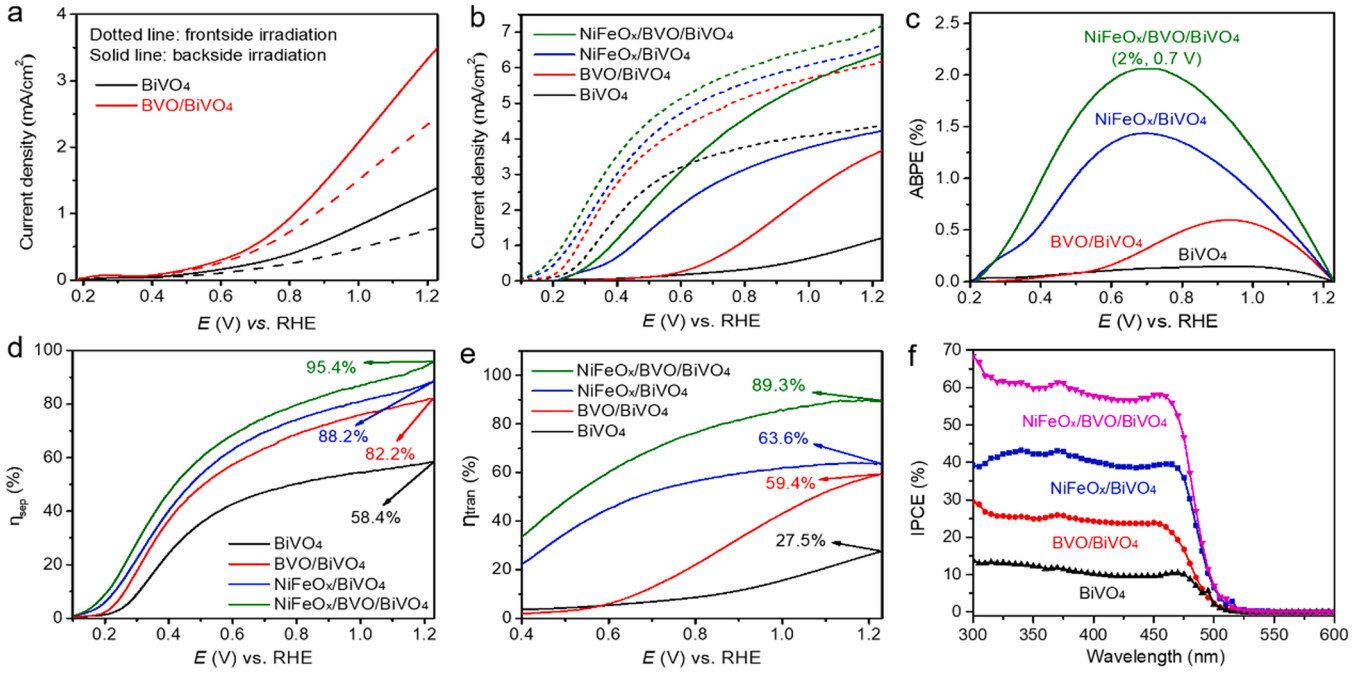

Fig. 3. (a) Photocurrent−potential (*J*−*V*) curves of $BiVO_4$ and $BVO/BiVO_4$. (b) *J*-*V* curves with and without Na_2SO_3 (the dotted line is with 0.5 M Na_2SO_3 solution), (c) Applied bias photon-to-current efficiencies, (d) Charge separation efficiency, (e) Charge transfer efficiencies, and (f) Incident photon-to-current efficiencies of four $BiVO_4$-based photoanodes. (The electrolyte is a 0.5 M borate buffer solution at a pH value of 9.5).

have been calculated and displayed in Fig. 3c. The maximum ABPE value of $NiFeO_x/BVO/BiVO_4$ sample can reach up to 2 % at 0.7 V, which is not only higher than those of $NiFeO_x/BiVO_4$ (1.4 %, 0.7 V) and $BVO/BiVO_4$ (0.6 %, 0.9 V), but also superior to most of the recently reported $BiVO_4$-based photoanodes [38–40]. Furthermore, the charge separation (η_{sep}) efficiencies and charge transfer (η_{tran}) efficiencies for PEC water oxidation was calculated, where Na_2SO_3 was used as holes sacrificial agent [41]. The pristine $BiVO_4$ exhibit a low η_{sep} value of 58.4 %, while the enhancement of (011)/(110) crystal plane and deposition of $NiFeO_x$ could effectively increase the η_{sep} up to 82.2 % and 95.4 %, respectively (Fig. 3d). The η_{tran} value of the $NiFeO_x/BVO/BiVO_4$ photoanode attains 89.3 % at 1.23 V, which is much higher than that of pristine $BiVO_4$ (27.5 %, 1.23 V), further augmenting that the enhancement of (011)/(110) crystal plane could enhance the charge separation (Fig. 3e). Moreover, the incident photon-to-current efficiency (IPCE) was performed at 1.23 V and 300–600 nm wavelengths to further understand the effect of (011) plane and $NiFeO_x$ on the photocurrent generation. The $NiFeO_x/BVO/BiVO_4$ photoanode reach its high IPCE value of 60 % at 470 nm, which is the significantly the highest among the $BVO/BiVO_4$, $NiFeO_x/BiVO_4$, and $BiVO_4$ photoanodes (Fig. 3f), and also indicating that $NiFeO_x/BVO/BiVO_4$ has more efficient extraction of charge carriers.

In addition to high efficiency, stability is another key factor for practical application of photoelectrodes [42,43]. The photochemical corrosion of $BiVO_4$ photoanode is thought to be caused by photogenic holes. A rich Bi oxide layer is formed on the surface and VO_4^{3-} is leached into the electrolyte [42]. To evaluate the stability of $NiFeO_x/BVO/BiVO_4$ sample, current density versus time curve measurement was performed at 0.7 V vs. RHE. As presented in Fig. 4a, the photocurrent density of $NiFeO_x/BVO/BiVO_4$ photoanode decreases slightly main an average density of 4.0 mA cm^{-2} at 0.7 V vs. RHE for 22 h, confirming the excellent stability. As can be observed in the illustration, a large number of bubbles form on the surface of the $NiFeO_x/BVO/BiVO_4$ photoanode. In contrast, the $BVO/BiVO_4$ photoanode displays a significant drop in photocurrent, especially in a short period of time (Fig. S5, Supporting Information). Such result reveals that $NiFeO_x$ functional layer can effectively improve the stability, mainly by preserving the phase and structure of the $NiFeO_x/BVO/BiVO_4$ catalyst (Fig. S6 and Fig. S7, Supporting Information) [44,45]. Moreover, the amount of H_2 and O_2 gases of $NiFeO_x/BVO/BiVO_4$ photoanode were measured at 1.23 V vs. RHE in a gas-tight PEC chamber equipped with a chromatograph (Fig. 4b). The *i-t* results for the hydrogen and oxygen generation at 1.23 V vs. RHE was provided in Fig. S8, revealing the excellent stability. The yield of O_2 and H_2 gases reached 857.4 and 429.6 μmol cm^{-2} in 6 h under simulated AM1.5 illumination (Fig. 4c), and the evolution rates reached a remarkable 142.9 and 71.6 μmol cm^{-2} h^{-1} (Fig. 4d), respectively.

3.3. Density functional theory (DFT) calculation

To ascertain the microscopic mechanism of the promotion effect of the (011)/(110) crystal plane on the PEC water oxidation, we performed density functional theory (DFT) calculations from the viewpoint of interfacial charge transfer and surface catalysis [12,46]. As depicted in Fig. 5a and Fig. S9 Supporting Information, H_2O cluster was placed on the (110) facet, (011) facet, and (110)/(011) facet of $BiVO_4$ to simulate the (110)/(011) facet interface and charge density. The density of states (DOS) of the (110), (011), and (110)/(011) facets of $BiVO_4$ were plotted to decipher the electronic interaction between the $BiVO_4$ and H_2O. Hence, the DOS across the Fermi level (E_f) for (110) facet and (011) facet are shown in Fig. 5b. After formation of (110)/(011) facet, the valence bands was modified, revealing stronger electronic interaction. Furthermore, Fig. 5c reveals that the adsorption free energy diagram of H_2O^* (ΔG_{H2O^*}) on the (110)/(011) facet is − 0.5 eV, which is much lower than that of (110) facet (−0.71 eV) and (011) facet (−0.60 eV), indicating that (110)/(011) facet has suitable and better H_2O adsorption ability. Fig. 5d presents the Gibb's free energy change diagram of the four elementary steps in the OER process on the surface of (110) facet, (011) facet, and (110)/(011) interface of $BiVO_4$. Based on the

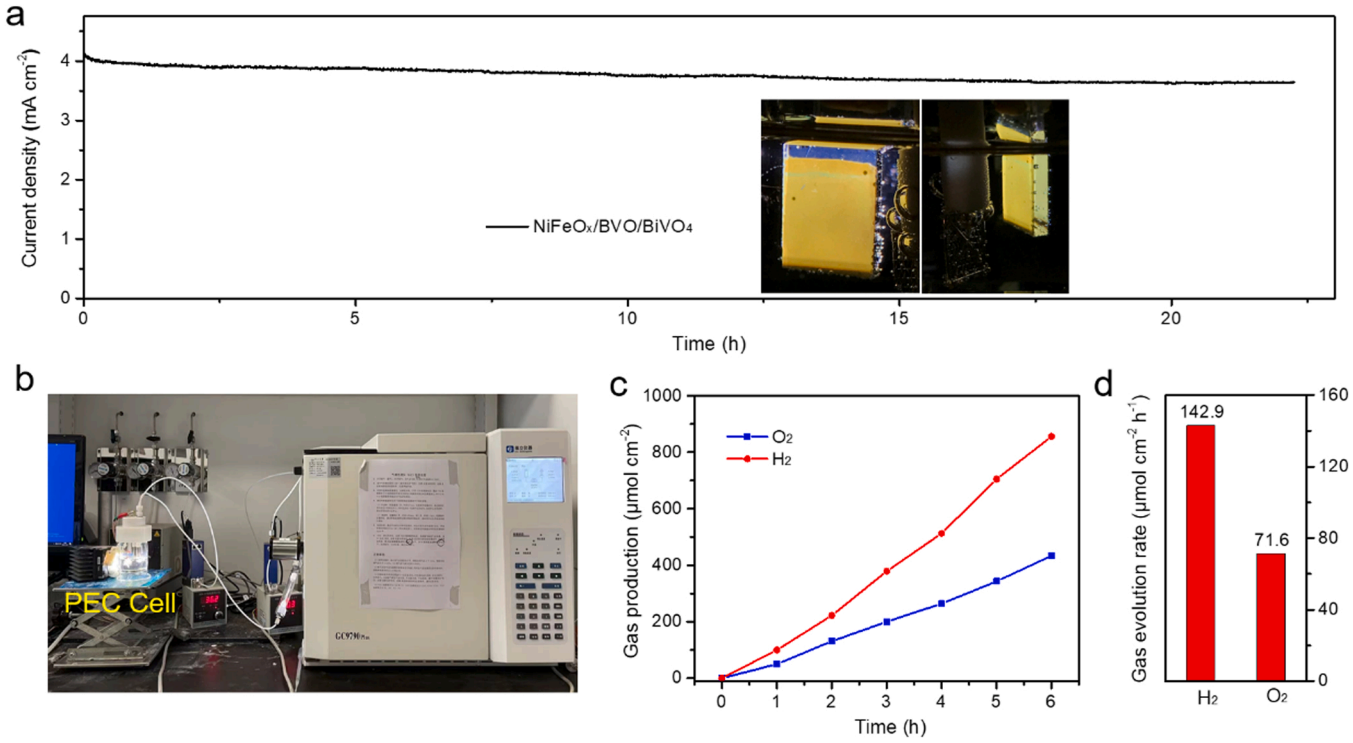

Fig. 4. (a) *J–T* curves of $NiFeO_x/BVO/BiVO_4$ photoanode at 0.7 V vs. RHE with 22 h (The illustration is the testing sample picture). (b) The photo-image of PEC cell and gas chromatography. (c) The production and (d) evolution rate of H_2 and O_2 with $NiFeO_x/BVO/BiVO_4$ photoanode at 1.23 V vs. RHE. (The electrolyte is a 0.5 M borate buffer solution at a pH value of 9.5).

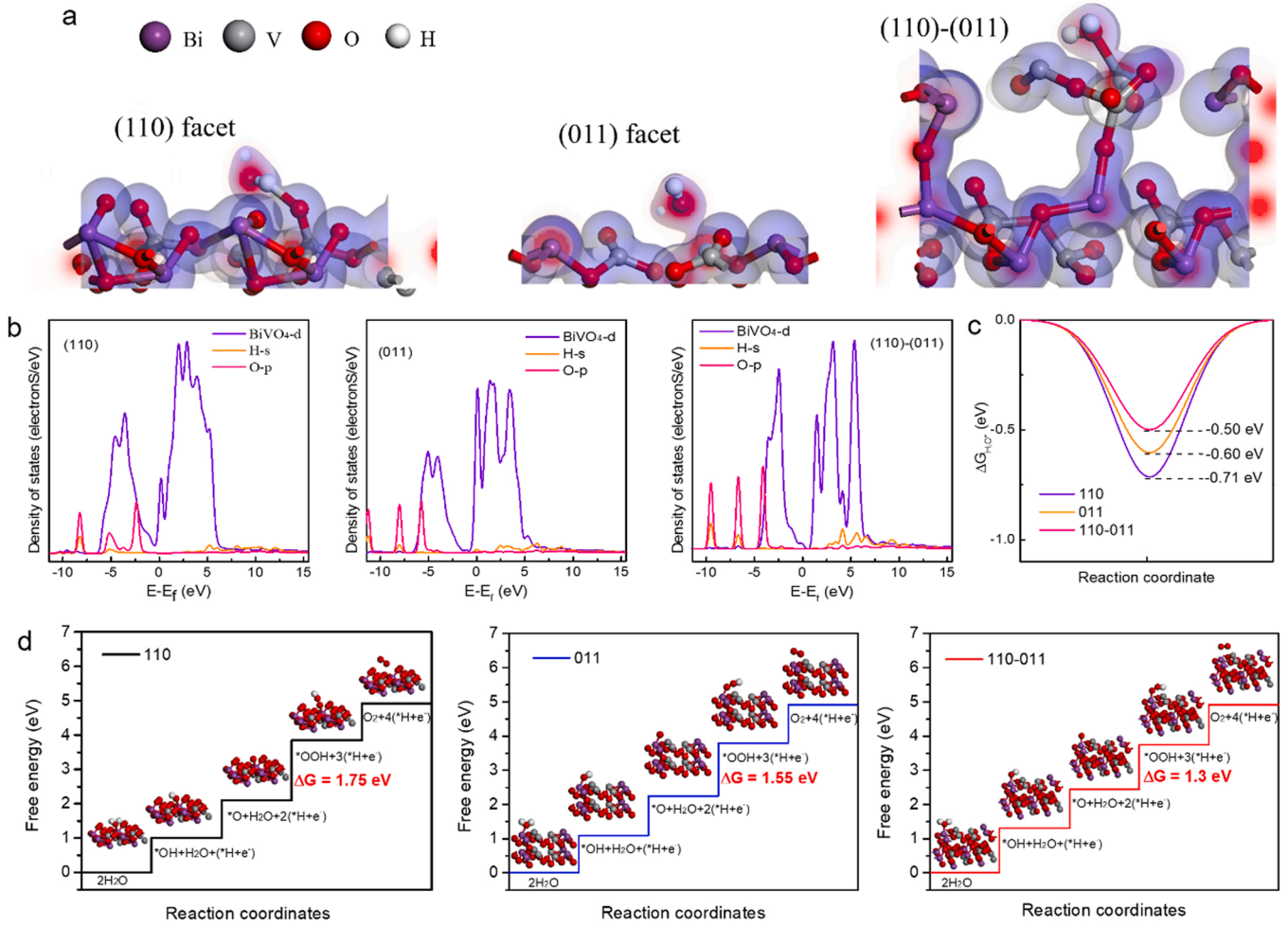

Fig. 5. (a) Visual representation of structures, (b) density of states, (c) the free-energy diagram (ΔG_{H2O*}), and (e) Free energy diagram of (110) facet, (011) facet, and (110)/(011) interface of $BiVO_4$.

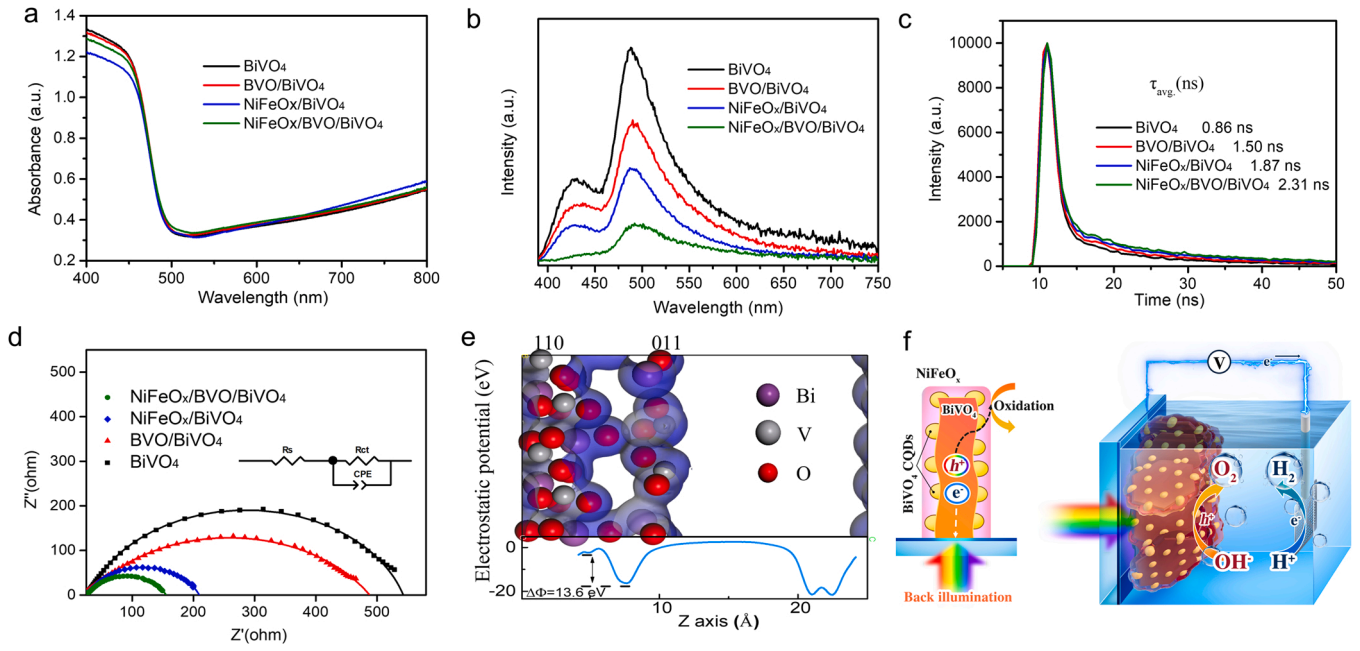

Fig. 6. (a) UV–vis spectra, (b) PL spectra with 325 nm excitation wavelength, (c) time-resolved transient photoluminescence, (d) electrochemical impedance spectra at 1.23 V vs RHE of four $BiVO_4$-based photoanodes (The electrolyte is a 0.5 M borate buffer solution at a pH value of 9.5). (e) Calculated electron density and electrostatic potentials of $NiFeO_x/BVO/BiVO_4$ photoanode. (f) Illustrations of the charge transfer process for $NiFeO_x/BVO/BiVO_4$ photoanode.

calculation results, (110) facet $BiVO_4$ presents the largest energy barrier (ΔG) of 1.75 eV with the formation of *OOH in the OER process, indicating the potential rate determining step [47]. While the low energy barrier of (011) facet with the determining step reaches 1.55 eV. However, at the homogenous interface of (110)/(011) facet, the rate determining step energy barrier substantially decreased to 1.3 eV, reveling that the (110)/(011) interface accelerates the reaction kinetics for PEC water oxidation.

3.4. Charge transfer analysis

To study the charge transfer dynamics and gain more insight into the role of the exposed (011) crystal facet and $NiFeO_x$ on the PEC water oxidation, a range of spectroscopic and electrochemical techniques were performed [22,48,49]. To begin with, the optical property of four photoanodes was evaluated by UV–vis absorption spectra in Fig. 6a, which shows a similar absorption edge at 520 nm, corresponding to visible light. It reveals that the deposited $BiVO_4$ nanodots with exposed (011) crystal facet and $NiFeO_x$ cocatalyst have not change the absorption ability, which excluded the effect of light harvesting efficiency on the PEC performance [50]. Furthermore, photoluminescence (PL) spectra were measured to study the charge transfer and separation. As presented in Fig. 6b, $BiVO_4$ sample shows a remarkable emission peak at 495 nm, which can be ascribed to the band-band PL phenomenon [51]. Compared to $BiVO_4$, the emission peak of $NiFeO_x$/BVO/$BiVO_4$ dramatically decreased, which may be due to the suppressed charge recombination. The time-resolved transient photoluminescence measurements were performed to study the photogenerated charge carrier kinetics. The average charge lifetimes values of $BiVO_4$, BVO/$BiVO_4$, NiFeOx/$BiVO_4$, and $NiFeO_x$/BVO/$BiVO_4$ are 0.86 ns, 1.50 ns, 1.87 ns and 2.31 ns, respectively (Fig. 6c and Table S2). The prolonged lifetime indicates that the effective utilization of holes in the photoanodes leads to charge separation. The enhanced interfacial charge transfer ability of $NiFeO_x$/BVO/$BiVO_4$ was further also confirmed by electrochemical impedance spectroscopy (EIS) results (Fig. 6d). The interface charge transfer resistance between the electrolyte and photoanodes (R_{ct}) was obtained based on the equivalent Randles circuit model (Table S3, Supporting Information). The $NiFeO_x$/BVO/$BiVO_4$ sample demonstrates the smallest semi-circle, indicating that it has the best electrical conductivity and interfacial charge transfer ability [39,52–54]. Additionally, the BVO/$BiVO_4$ homojunction with (011) crystal plane effectively boosted the interfacial charge transfer ability. The calculation shows that the electron density increases in the region of the (001) crystal plane (blue part), revealing that (001) crystal plane effectively promotes the charge transport (Fig. 6e). Based on the above analysis, the synergistic effect between $BiVO_4$ nanodots with exposed (011) crystal facet and $NiFeO_x$ cocatalyst can enhance the performance of PEC water oxidation by strengthening electron transport. Therefore, the enhanced PEC water oxidation performance of $NiFeO_x$/BVO/$BiVO_4$ photoanode can be ascribed to the following aspects (Fig. 6f): I) Accelerated charge separation owing to the sufficient and strong coupling interfaces in the BVO/$BiVO_4$ homojunction; II) Conducive charge transportation to the electrode surface owing to the formation of the $BiVO_4$ nanodots with exposed (011) crystal facet; III) Enhanced stability and reaction kinetics for PEC water oxidation owing to the incorporation of the ultrathin $NiFeO_x$ layer.

4. Conclusions

In summary, an excellent $NiFeO_x$/BVO/$BiVO_4$ photoanode for photoelectrochemical water splitting has been successfully fabricated. The PEC activity of $BiVO_4$ has been drastically increased by the sequential electroplating of two functional materials, namely BVO nanodots and $NiFeO_x$. The superior photocurrent density of $NiFeO_x$/BVO/$BiVO_4$ photoanode reaches 6.40 mA cm^{-2} at 1.23 V vs. RHE under simulated AM 1.5G solar illumination, which is 4.7 times higher compared to pristine $BiVO_4$ (1.37 mA cm^{-2}). Additionally, $NiFeO_x$/BVO/$BiVO_4$ photoanode exhibits enhancement of photocorrosion resistance. A comprehensive analysis, including theoretical calculations and experimental measurements, shows that the BVO nanodots are favorable for charge transport, whereas $NiFeO_x$ passivate holes trap states, which significantly reduce the surface electron recombination and strengthen holes injection, thus improving water splitting. This unique discovery provides a promising strategy for tuning $BiVO_4$ photoanodes with functional interlayers towards enhancing charge separation and achieving superior PEC performance.

CRediT authorship contribution statement

Zifei Xie: Experiment, Data processing & analysis, Writing – original draft. **Daoming Chen:** Investigation, Data analysis, Revised manuscript preparation. **Jingtong Zhai:** Investigation, Data analysis, Revised manuscript preparation. **Yongchao Huang:** Formal analysis, Writing – review & editing, Resources. **Hongbing Ji:** Formal analysis, Writing – review & editing.

Declaration of Competing Interest

The authors declare that they have no known competing financial interests or personal relationships that could have appeared to influence the work reported in this paper.

Data Availability

Data will be made available on request.

Acknowledgements

Natural Science Foundation of Guangzhou (202201020147) and Innovation Training Program for College Students of Guangzhou University (202211078133).

Appendix A. Supporting information

Supplementary data associated with this article can be found in the online version at doi:10.1016/j.apcatb.2023.122865.

References

[1] V. Andrei, R.A. Jagt, M. Rahaman, L. Lari, V.K. Lazarov, J.L. MacManus-Driscoll, R. L.Z. Hoye, E. Reisner, Long-term solar water and CO_2 splitting with photoelectrochemical BiOI–$BiVO_4$ tandems, Nat. Mater. 21 (2022) 864–868.
[2] S. Ye, W. Shi, Y. Liu, D. Li, H. Yin, H. Chi, Y. Luo, N. Ta, F. Fan, X. Wang, C. Li, Unassisted photoelectrochemical cell with multimediator modulation for solar water splitting exceeding 4 % solar-to-hydrogen efficiency, J. Am. Chem. Soc. 143 (2021) 12499–12508.
[3] B. Moss, Q. Wang, K.T. Butler, R. Grau-Crespo, S. Selim, A. Regoutz, T. Hisatomi, R. Godin, D.J. Payne, A. Kafizas, K. Domen, L. Steier, J.R. Durrant, Linking in situ charge accumulation to electronic structure in doped $SrTiO_3$ reveals design principles for hydrogen-evolving photocatalysts, Nat. Mater. 20 (2021) 511–517.
[4] T. Xiong, B. Huang, J. Wei, X. Yao, R. Xiao, Z. Zhu, F. Yang, Y. Huang, H. Yang, M. S. Balogun, Unveiling the promotion of accelerated water dissociation kinetics on the hydrogen evolution catalysis of $NiMoO_4$ nanorods, J. Energy Chem. 67 (2022) 805–813.
[5] T. Xiong, X. Yao, Z. Zhu, R. Xiao, Y.-w Hu, Y. Huang, S. Zhang, M.-S. Balogun, In situ grown Co-based interstitial compounds: non-3d metal and non-metal dual modulation boosts alkaline and acidic hydrogen electrocatalysis, Small 18 (2022), 2105331.
[6] T. Higashi, H. Nishiyama, V. Nandal, Y. Pihosh, Y. Kawase, R. Shoji, M. Nakabayashi, Y. Sasaki, N. Shibata, H. Matsuzaki, K. Seki, K. Takanabe, K. Domen, Design of semitransparent tantalum nitride photoanode for efficient and durable solar water splitting, Energy Environ. Sci. 15 (2022) 4761–4775.
[7] D. Dai, X. Liang, B. Zhang, Y. Wang, Q. Wu, X. Bao, Z. Wang, Z. Zheng, H. Cheng, Y. Dai, B. Huang, P. Wang, Strain adjustment realizes the photocatalytic overall water splitting on tetragonal zircon $BiVO_4$, Adv. Sci. 9 (2022), 2105299.
[8] Z. Wang, Y. Guo, M. Liu, X. Liu, H. Zhang, W. Jiang, P. Wang, Z. Zheng, Y. Liu, H. Cheng, Y. Dai, Z. Wang, B. Huang, Boosting H_2 production from a $BiVO_4$ photoelectrochemical biomass fuel cell by the construction of a bridge for charge and energy transfer, Adv. Mater. 34 (2022), 2201594.

[9] Y. Lu, Y. Yang, X. Fan, Y. Li, D. Zhou, B. Cai, L. Wang, K. Fan, K. Zhang, Boosting charge transport in $BiVO_4$ photoanode for solar water oxidation, Adv. Mater. 34 (2022), 2108178.

[10] R.-T. Gao, X. Guo, S. Liu, X. Zhang, X. Liu, Y. Su, L. Wang, Ultrastable and high-performance seawater-based photoelectrolysis system for solar hydrogen generation, Appl. Catal. B Environ. 304 (2022), 120883.

[11] T.W. Kim, K.-S. Choi, Nanoporous $BiVO_4$ photoanodes with dual-layer oxygen evolution catalysts for solar water splitting, Science 343 (2014) 990–994.

[12] V. Andrei, G.M. Ucoski, C. Pornrungroj, C. Uswachoke, Q. Wang, D.S. Achilleos, H. Kasap, K.P. Sokol, R.A. Jagt, H. Lu, T. Lawson, A. Wagner, S.D. Pike, D. S. Wright, R.L.Z. Hoye, J.L. MacManus-Driscoll, H.J. Joyce, R.H. Friend, E. Reisner, Floating perovskite-$BiVO_4$ devices for scalable solar fuel production, Nature 608 (2022) 518–522.

[13] Y. Wang, J. Zhang, M.S. Balogun, Y. Tong, Y. Huang, Oxygen vacancy–based metal oxides photoanodes in photoelectrochemical water splitting, Mater. Today Sustain. 18 (2022), 100118.

[14] S. Sun, W. Wang, D. Li, L. Zhang, D. Jiang, Solar light driven pure water splitting on quantum sized $BiVO_4$ without any cocatalyst, ACS Catal. 4 (2014) 3498–3503.

[15] R. Li, H. Han, F. Zhang, D. Wang, C. Li, Highly efficient photocatalysts constructed by rational assembly of dual-cocatalysts separately on different facets of $BiVO_4$, Energy Environ. Sci. 7 (2014) 1369–1376.

[16] S. Heckel, C. Bilsing, M. Wittmann, T. Gemming, L. Büttner, J. Czarske, J. Simmchen, Beyond Janus geometry: characterization of flow fields around nonspherical photocatalytic microswimmers, Adv. Sci. 9 (2022), 2105009.

[17] R. Li, F. Zhang, D. Wang, J. Yang, M. Li, J. Zhu, X. Zhou, H. Han, C. Li, Spatial separation of photogenerated electrons and holes among {010} and {110} crystal facets of $BiVO_4$, Nat. Commun. 4 (2013) 1432.

[18] F. Wang, J. Zhang, C.-C. Jin, X. Ke, F. Wang, D. Liu, Unveiling the effect of crystal facets on piezo-photocatalytic activity of $BiVO_4$, Nano Energy 101 (2022), 107573.

[19] Y. Miao, J. Liu, L. Chen, H. Sun, R. Zhang, J. Guo, M. Shao, Single-atomic-Co cocatalyst on (040) facet of $BiVO_4$ toward efficient photoelectrochemical water splitting, Chem. Eng. J. 427 (2022), 131011.

[20] Y. Qi, J. Zhang, Y. Kong, Y. Zhao, S. Chen, D. Li, W. Liu, Y. Chen, T. Xie, J. Cui, C. Li, K. Domen, F. Zhang, Unraveling of cocatalysts photodeposited selectively on facets of $BiVO_4$ to boost solar water splitting, Nat. Commun. 13 (2022) 484.

[21] C.-C. Lai, J.-W. Chen, J.-C. Chang, C.-Y. Kuo, Y.-C. Liu, J.-C. Yang, Y.-T. Hsieh, S.-W. Tseng, Y.-C. Pu, Two-step process of a crystal facet-modulated $BiVO_4$ photoanode for efficiency improvement in photoelectrochemical hydrogen evolution, ACS Appl. Mater. Interfaces 14 (2022) 24919–24928.

[22] C.W. Kim, Y.S. Son, M.J. Kang, D.Y. Kim, Y.S. Kang, (040)-crystal facet engineering of $BiVO_4$ plate photoanodes for solar fuel production, Adv. Energy Mater. 6 (2016), 1501754.

[23] D. Li, Y. Liu, W. Shi, C. Shao, S. Wang, C. Ding, T. Liu, F. Fan, J. Shi, C. Li, Crystallographic-orientation-dependent charge separation of $BiVO_4$ for solar water oxidation, ACS Energy Let. 4 (2019) 825–831.

[24] J. Su, Z. Bai, B. Huang, X. Quan, G. Chen, Unique three dimensional architecture using a metal-free semiconductor cross-linked bismuth vanadate for efficient photoelectrochemical water oxidation, Nano Energy 24 (2016) 148–157.

[25] B. Zhang, H. Zhang, Z. Wang, X. Zhang, X. Qin, Y. Dai, Y. Liu, P. Wang, Y. Li, B. Huang, Doping strategy to promote the charge separation in $BiVO_4$ photoanodes, Appl. Catal. B Environ. 211 (2017) 258–265.

[26] M. Zhong, T. Hisatomi, Y. Kuang, J. Zhao, M. Liu, A. Iwase, Q. Jia, H. Nishiyama, T. Minegishi, M. Nakabayashi, N. Shibata, R. Niishiro, C. Katayama, H. Shibano, M. Katayama, A. Kudo, T. Yamada, K. Domen, Surface modification of CoO_x loaded $BiVO_4$ photoanodes with ultrathin p-type NiO layers for improved solar water oxidation, J. Am. Chem. Soc. 137 (2015) 5053–5060.

[27] X. Chang, T. Wang, P. Zhang, J. Zhang, A. Li, J. Gong, Enhanced surface reaction kinetics and charge separation of p–n heterojunction $Co_3O_4/BiVO_4$ photoanodes, J. Am. Chem. Soc. 137 (2015) 8356–8359.

[28] B. Jin, Y. Cho, C. Park, J. Jeong, S. Kim, J. Jin, W. Kim, L. Wang, S. Lu, S. Zhang, S. H. Oh, K. Zhang, J.H. Park, A two-photon tandem black phosphorus quantum dot-sensitized $BiVO_4$ photoanode for solar water splitting, Energy Environ. Sci. 15 (2022) 672–679.

[29] K.-H. Ye, Z. Wang, J. Gu, S. Xiao, Y. Yuan, Y. Zhu, Y. Zhang, W. Mai, S. Yang, Carbon quantum dots as a visible light sensitizer to significantly increase the solar water splitting performance of bismuth vanadate photoanodes, Energy Environ. Sci. 10 (2017) 772–779.

[30] M.G. Lee, D.H. Kim, W. Sohn, C.W. Moon, H. Park, S. Lee, H.W. Jang, Conformally coated $BiVO_4$ nanodots on porosity-controlled WO_3 nanorods as highly efficient type II heterojunction photoanodes for water oxidation, Nano Energy 28 (2016) 250–260.

[31] J. Zhang, Y. Huang, X. Lu, J. Yang, Y. Tong, Enhanced $BiVO_4$ photoanode photoelectrochemical performance via borate treatment and a $NiFeO_x$ cocatalyst, ACS Sustain. Chem. Eng. 9 (2021) 8306–8314.

[32] Y.J. Jeong, D.H. Seo, Jh Baek, M.J. Kang, B.N. Kim, Sk Kim, X. Zheng, I.S. Cho, Crystal reconstruction of Mo:$BiVO_4$: improved charge transport for efficient solar water splitting, Adv. Funct. Mater. 32 (2022), 2208196.

[33] D. Lee, W. Wang, C. Zhou, X. Tong, M. Liu, G. Galli, K.-S. Choi, The impact of surface composition on the interfacial energetics and photoelectrochemical properties of $BiVO_4$, Nat. Energy 6 (2021) 287–294.

[34] X. Lu, K.-h Ye, S. Zhang, J. Zhang, J. Yang, Y. Huang, H. Ji, Amorphous type FeOOH modified defective $BiVO_4$ photoanodes for photoelectrochemical water oxidation, Chem. Eng. J. 428 (2022), 131027.

[35] Y. Huang, H. Li, M.-S. Balogun, W. Liu, Y. Tong, X. Lu, H. Ji, Oxygen vacancy induced bismuth oxyiodide with remarkably increased visible-light absorption and superior photocatalytic performance, ACS Appl. Mater. Interfaces 6 (2014) 22920–22927.

[36] C. Zachäus, F.F. Abdi, L.M. Peter, R. van de Krol, Photocurrent of $BiVO_4$ is limited by surface recombination, not surface catalysis, Chem. Sci. 8 (2017) 3712–3719.

[37] R.-T. Gao, S. Liu, X. Guo, R. Zhang, J. He, X. Liu, T. Nakajima, X. Zhang, L. Wang, Pt-induced defects curing on $BiVO_4$ photoanodes for near-threshold charge separation, Adv. Energy Mater. 11 (2021), 2102384.

[38] S. Zhou, K. Chen, J. Huang, L. Wang, M. Zhang, B. Bai, H. Liu, Q. Wang, Preparation of heterometallic CoNi-MOFs-modified $BiVO_4$: a steady photoanode for improved performance in photoelectrochemical water splitting, Appl. Catal. B Environ. 266 (2020), 118513.

[39] L. Hu, Y. Hu, R. Liu, Y. Mao, M.S. Balogun, Y. Tong, Co-based MOF-derived Co/CoN/Co_2P ternary composite embedded in N- and P-doped carbon as bifunctional nanocatalysts for efficient overall water splitting, Int. J. Hydrogen Energy 44 (2019) 11402–11410.

[40] Q. Meng, B. Zhang, L. Fan, H. Liu, M. Valvo, K. Edström, M. Cuartero, R. de Marco, G.A. Crespo, L. Sun, Efficient $BiVO_4$ photoanodes by postsynthetic treatment: remarkable improvements in photoelectrochemical performance from facile borate modification, Angew. Chem. Int. Ed. 58 (2019) 19027–19033.

[41] R.-T. Gao, D. He, L. Wu, K. Hu, X. Liu, Y. Su, L. Wang, Towards long-term photostability of nickel hydroxide/$BiVO_4$ photoanodes for oxygen evolution catalysts via in-situ catalyst tuning, Angew. Chem. Int. Ed. 59 (2020) 6213–6218.

[42] D.K. Lee, K.-S. Choi, Enhancing long-term photostability of $BiVO_4$ photoanodes for solar water splitting by tuning electrolyte composition, Nat. Energy 3 (2018) 53–60.

[43] B. Zhang, L. Wang, Y. Zhang, Y. Ding, Y. Bi, Ultrathin FeOOH nanolayers with abundant oxygen vacancies on $BiVO_4$ photoanodes for efficient water oxidation, Angew. Chem. Int. Ed. 57 (2018) 2248–2252.

[44] J.-B. Pan, B.-H. Wang, J.-B. Wang, H.-Z. Ding, W. Zhou, X. Liu, J.-R. Zhang, S. Shen, J.-K. Guo, L. Chen, C.-T. Au, L.-L. Jiang, S.-F. Yin, Activity and stability boosting of an oxygen-vacancy-rich $BiVO_4$ photoanode by NiFe-MOFs thin layer for water oxidation, Angew. Chem. Int. Ed. 60 (2021) 1433–1440.

[45] B. Zhang, S. Yu, Y. Dai, X. Huang, L. Chou, G. Lu, G. Dong, Y. Bi, Nitrogen-incorporation activates $NiFeO_x$ catalysts for efficiently boosting oxygen evolution activity and stability of $BiVO_4$ photoanodes, Nat. Commun. 12 (2021) 6969.

[46] Q. Zhang, M. Liu, W. Zhou, Y. Zhang, W. Hao, Y. Kuang, H. Liu, D. Wang, L. Liu, J. Ye, A novel Cl- modification approach to develop highly efficient photocatalytic oxygen evolution over $BiVO_4$ with AQE of 34.6 %, Nano Energy 81 (2021), 105651.

[47] A. Venugopal, R. Kas, K. Hau, W.A. Smith, Operando infrared spectroscopy reveals the dynamic nature of semiconductor–electrolyte interface in multinary metal oxide photoelectrodes, J. Am. Chem. Soc. 143 (2021) 18581–18591.

[48] J. Xiao, F. Zhao, J. Zhong, Z. Huang, L. Fan, L. Peng, S.-F. Zhou, G. Zhan, Performance enhancement of hematite photoanode with oxygen defects for water splitting, Chem. Eng. J. 402 (2020), 126163.

[49] K.-H. Ye, Z. Chai, J. Gu, X. Yu, C. Zhao, Y. Zhang, W. Mai, BiOI–$BiVO_4$ photoanodes with significantly improved solar water splitting capability: p–n junction to expand solar adsorption range and facilitate charge carrier dynamics, Nano Energy 18 (2015) 222–231.

[50] S. Ju, H. Kang, J. Jun, S. Son, J. Park, W. Kim, H. Lee, Periodic micropillar-patterned FTO/$BiVO_4$ with superior light absorption and separation efficiency for efficient PEC performance, Small 17 (2021), 2006558.

[51] J. Xiao, L. Fan, F. Zhao, Z. Huang, S.-F. Zhou, G. Zhan, Kinetic analysis of the synergistic effect of NaBH4 treatment and Co-Pi coating on Fe_2O_3 photoanodes for photoelectrochemical water oxidation, J. Catal. 381 (2020) 139–149.

[52] S.S. Kalanur, H. Seo, Work function tuned, surface Cs intercalated $BiVO_4$ for enhanced photoelectrochemical water splitting reactions, J. Energy Chem. 68 (2022) 612–623.

[53] W. Zhang, F. Wu, J. Li, D. Yan, J. Tao, Y. Ping, M. Liu, Unconventional relation between charge transport and photocurrent via boosting small polaron hopping for photoelectrochemical water splitting, ACS Energy Lett. 3 (2018) 2232–2239.

[54] R. Xiao, P. Huang, T. Xiong, J. Wei, F. Wang, J. Deng, Z. Wang, M.S. Balogun, Advanced trifunctional electrodes for 1.5 V-based self-powered aqueous electrochemical energy devices, J. Mater. Chem. A 11 (2023) 374–384.